Check for updates

Black TiO$_2$ nanotube arrays fabricated by electrochemical self-doping and their photoelectrochemical performance

Liyan Zhu, Hongchao Ma, [ID]†* Huibin Han, Yinghuan Fu,†* Chun Ma, Zhihui Yu and Xiaoli Dong

Herein, black TiO$_2$ nanotube arrays (NTAs) were fabricated using electrochemical self-doping approaches, and characterized systemically by scanning electron microscopy (SEM), powder X-ray diffraction (XRD), UV-visible absorption spectroscopy and photoluminescence spectroscopy (PL). The as-obtained black TiO$_2$ nanotube arrays (NTAs) exhibited stronger absorption in the visible-light region, a better separation rate of light-induced carriers, and higher electrical conductivity than TiO$_2$ nanotube arrays (NTAs). These characteristics cause black TiO$_2$ nanotube array (NTA) electrodes to have higher photoelectrocatalytic activity for degrading anthraquinone dye (reactive brilliant blue KN-R) than the TiO$_2$ nanotube array (NTA) electrode. Furthermore, a synergetic action between photocatalysis and electrocatalysis was also observed. The black TiO$_2$ nanotube array (NTA) electrode is considered to be a promising photoanode for the treatment of organic pollutants.

1. Introduction

Recently, TiO$_2$-based active materials (especially, TiO$_2$ nanotube arrays (NTAs)) have attracted a great deal of attention for the photocatalytic/photoelectrocatalytic degradation of organic pollutants, and energy storage, because their ordered nanotube architecture can provide a unidirectional electric channel for the photogenerated electrons, a large internal surface area, and high ion changeability.[1–7] However, some problems associated with their wide band gap (3.0–3.2 eV) and the fast recombination of photogenerated carriers still needs to be solved to enable practical application of TiO$_2$ NTAs.

More effort has been made to enhance the light absorption, and to suppress the recombination of electron/hole pairs, such as, doping (non-metal and metal elements),[8–12] noble metal particle decoration,[13–18] and heterostructure construction.[19–21] Other than the above strategies, photoelectrocatalysis (PEC) has received the most attention as a facile and efficient route to overcome the fast recombination between the photoinduced carriers in TiO$_2$ NTAs.[22,23] During the PEC process, a low positive bias was applied to the TiO$_2$ NTAs, which significantly facilitated the transfer of photocarriers and improved the separation of the photoinduced carriers. However, it should be noted that the electrooxidation features of TiO$_2$ NTAs for the degradation

of organic pollutants have not attracted more attention, which may be attributed to their semiconducting nature and poor electronic conductivity. Thus, the development of methods to improve the electrocatalytic performance of TiO$_2$ NTAs, to achieve synergy between photocatalysis and electrocatalysis, and to enhance the photoelectrocatalytic ability of TiO$_2$ NTAs has become a significant challenge in the field of environmental remediation.

In recent years, reduced titanium oxide (or black TiO$_2$) has attracted increasing attention for use in photovoltaics and photocatalysis, due to its narrower bandgap and higher electrical conductivity.[24–26] Some reports indicated that reduced TiO$_2$ NTAs not only exhibited excellent photocatalytic activity, but also demonstrated capacitive/oxidant generating properties due to the self-doping of TiO$_2$ with Ti^{3+}/oxygen vacancies.[27–30] Therefore, reduced TiO$_2$ NTAs are considered to be a promising photoanode material to achieve synergetic photoelectrochemical action in the PEC process. Nevertheless, thus far no information has been reported regarding their electrooxidation or PEC properties in the degradation of organic pollutants. Previous reports have mainly focused on electro-assisted photocatalytic processes of photocatalysts, in which electro-oxidation does not occur; only a few have focused on the electrooxidation processes during the PEC process. Thus, the aim of present work was to integrate the photooxidation and electrooxidation for black TiO$_2$ NTAs as photoanode in the PEC degradation of organic pollutants. Our results indicated that the efficient removal of organic pollutants over the black TiO$_2$ NTAs photoanode can be ascribed to the synergetic action between photocatalysis and electrocatalysis in the PEC process.

School of Light Industry & Chemical Engineering, Dalian Polytechnic University, No. 1 Qinggongyuan, Ganjingzi District, Dalian, P. R. China. E-mail: m-h-c@sohu.com; fuyinghuan@sina.com; Fax: (+86)-411-86323736; Tel: (+86)-411-86323508

† School of Chemistry Engineering & Material, Dalian Polytechnic University, No. 1 Qinggongyuan, Ganjingzi District, Dalian 116034, P. R. China.

2. Experimental section

2.1 Materials

Titanium sheets (99.7% pure) were obtained from Yunjie Metal Company (China). The ethylene glycol, acetone, ethanol, sodium sulfate, NH_4F, and reactive brilliant blue KN-R (from Tianjin Chemical Reagents Company) were of analytical grade. Deionized water was used as a solvent to prepare all solutions.

2.2 Preparation of pristine TiO$_2$ nanotube arrays

First, Ti sheets (10 mm × 10 mm × 1 mm in size) were cleaned in acetone and ethanol under ultrasonication, subsequently immersed in an aqueous oxalic acid solution (10%, 80 °C) for 2 h, and then washed using deionized water. A pretreated Ti sheet was used as the anode and an untreated Ti sheet was used as the cathode. The electrode sheets were placed vertically with a separation of 30 mm in an ethylene glycol electrolyte containing H_2O (5 wt%) and NH_4F (0.27 wt%) under a constant potential (40 V) for 2 h at room temperature (25 °C). Subsequently, the as-anodized TiO_2 NTAs were washed in ethanol for 10 min and calcined at 400 °C for 2 h under ambient conditions.

2.3 Preparation of black TiO$_2$ nanotube arrays

Preparation of black TiO_2 was performed using the electrochemical doping procedure suggested in ref. 31. In a typical procedure, the as-obtained pristine TiO_2 NTAs were used as the cathode, and a Ti sheet with the same area was selected as the counter electrode. To obtain the black TiO_2 NTAs, electrochemical reduction was performed at a set voltage (−30, −35, −40, −45 and −50 V) for a certain time (15, 20, 30, 60 and 120 min) in an ethylene glycol solution containing H_2O (5 wt%) and NH_4F (0.27 wt%).

2.4 Activity test

The degradation of reactive brilliant blue KN-R in an aqueous solution with a concentration of 60 mg L^{-1} (200 mL of solution with 0.1 M Na_2SO_4 as a supporting electrolyte) in a quartz reactor was used to evaluate the photo-electrocatalytic activity of the electrodes. The black TiO_2 NTAs anode and the titanium sheet cathode were immersed vertically in the solution, with a distance of 3 cm between the electrodes. Before the experiments, an adsorption–desorption equilibrium of the dye on the surface of the electrodes was established by magnetic stirring for 30 min under dark conditions. Electrochemical degradation was performed using a DC power supply, and a 175 W xenon lamp was selected as the light-source for the photocatalytic procedure. The xenon lamp was placed in a circulating water jacket to cool the reaction vessel. The reaction solution was sampled at given time intervals and centrifuged to remove the photocatalyst particles. A UV-visible spectrophotometer (UV-1800PC, MAPADA, China) was used for measuring the absorbance of solution and the degradation rate (R_0) of KN-R was estimated by the following equation:

$$R_0 = (A_0 - A_t)/A_0 \times 100\%$$

A_0 was the absorbance of initial solution of reactive brilliant blue KN-R and A_t was the absorbance of the solution of KN-R at time t.

2.5 Characterizations

Electrochemical tests were carried out using a CHI 660E potentiostat/galvanostat (ChenHua Instruments Co. Shanghai, China) with a standard three-electrode system. A platinum sheet and a saturated calomel electrode were selected as counter and reference electrodes. The morphologies of the samples were observed using a Hitachi-1510 scanning electron microscope (SEM) (Hitachi, Japan). X-Ray Diffraction (XRD) of the electrodes was performed using a SHIMADZU XRD-6100 X-ray diffractometer with Cu Kα radiation ($\lambda = 0.15406$ nm) at 40 kV and 30 mA. X-Ray photoelectron spectroscopy (XPS) experiments were carried out using a VG EscaLab 250 electron spectrometer (Thermo VG) with Al Kα X-ray radiation (1486.6 eV). The calibration of the binding energies was performed using the C 1s peak (284.6 eV). The UV-vis absorption spectra of the electrodes were obtained using a spectrophotometer (Varian Cary-100) with $BaSO_4$ as a standard. In this work, the fluorescence spectrophotometry was used to measure the amount of hydroxyl radical (˙OH) originating from the photo-electrocatalytic process.[32–34] The fluorescence experiments were carried out using a fluorescence spectrophotometer (Hitachi F-7000, Japan).

3. Results and discussion

Fig. 1 shows the XRD patterns of the black TiO_2-NTAs as a function of electrochemical reduction times and voltages. For reference, the XRD pattern of the TiO_2-NTAs is also included. As shown in Fig. 1, all the diffraction peaks of the TiO_2-NTAs matched well with the anatase phase of TiO_2 (JCPDS file no 21-1272) and with metallic Ti (JCPDS file no. 44-1294). No obvious change to the diffraction peaks of the pristine TiO_2-NTAs was observed after electrochemical reduction. The crystal structure of the pristine TiO_2-NTAs (crystalline anatase TiO_2) was also unchanged by the electrochemical reduction. Nevertheless, the XPS spectra of the pristine TiO_2 NTAs and black TiO_2 NTAs (see Fig. 1c) exhibited visible differences. The positions of the Ti 2p and O 1s peaks for the black TiO_2 NTAs are shifted to lower binding energy than that of the pristine TiO_2 NTAs. The negative shift in binding energy of the black TiO_2 NTAs can be attributed to the increased presence of Ti^{3+} and oxygen vacancies compared with pristine TiO_2 NTAs.[29,35] Fig. 1d shows the UV-Vis absorption spectra of the TiO_2 NTAs and black TiO_2 NTAs samples. The inset of Fig. 1d showed that the pristine TiO_2 NTAs is gray color, and its corresponding coloration is blue-black color after cathodic polarization. The pristine TiO_2 NTAs showed intrinsic absorption of TiO_2 at wavelengths below 400 nm. The visible-light absorption of the TiO_2 NTAs may be ascribed to the light scattering caused by pores or cracks in the nanotube arrays.[36–38] In contrast, the black TiO_2 NTAs sample exhibited stronger light-absorption than the pristine TiO_2 NTAs over the entire ultraviolet-visible region. Additionally, a notable
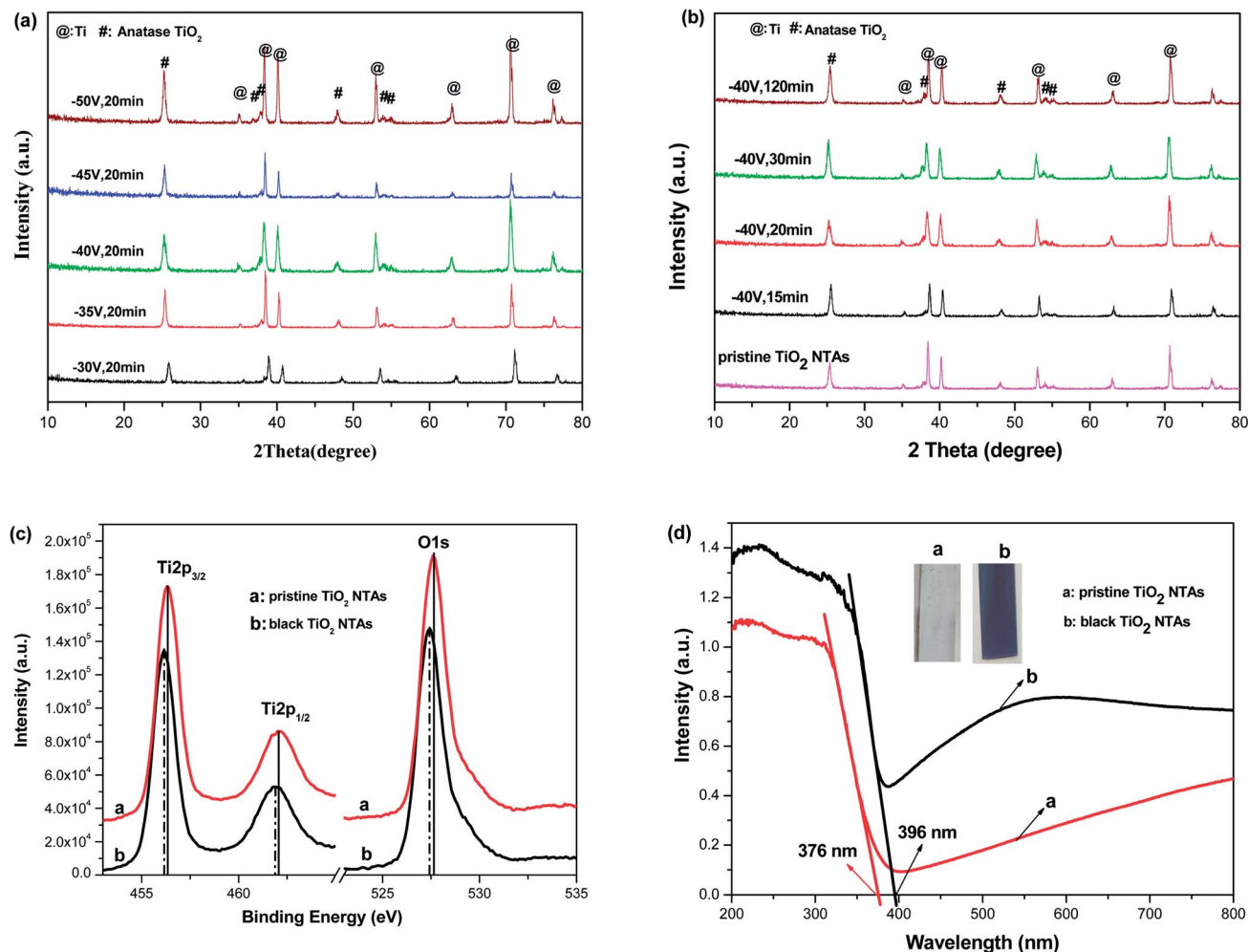
Fig. 1 XRD patterns of black TiO_2 NTAs prepared by electrochemical reduction under various reducing potential (a) and time (b); XPS (c) and UV–visible absorption spectra (d) of the pristine TiO_2 NTAs and black TiO_2 NTAs samples.

red shift was observed for the black TiO_2 NTAs. The absorption edge of the black TiO_2 NTAs was shifted to 396 nm, whereas the TiO_2 NTAs exhibited an absorption edge of 376 nm. The black TiO_2 NTAs also showed an additional absorption peak from 400 nm to the near-infrared region. Obviously, the distinct differences between optical absorption behavior of the TiO_2 NTAs and black TiO_2 NTAs samples may be correlated with the presence of vacancies (Ti^{3+} sites formed by cathodic polarization[39,40]) as a result of a trap state.[41,42] These results are also in agreement with those of previous studies.[27,43–45] Nevertheless, the strong light-absorption of the black TiO_2 NTAs is beneficial to improve their photocatalytic performance.

In order to identify the effect of electrochemical reduction on the morphology and structure of the TiO_2-NTAs, SEM measurement was performed (see Fig. 2). Fig. 2 shows that the TiO_2 NTAs had a regular nanotube-structure with a pore diameter of *ca.* 100 nm, and a length and wall thickness of about 20 nm and 1.0 μm, respectively. The diameter and length of the TiO_2 nanotubes did not change after electrochemical reduction. However, apparent damage to the pore structure of the TiO_2 NTAs was observed when the reduction time and

potential were increased to 20 min at −50 V and 60 min at −40 V. The damage to the pore structure should result in a decrease of electrocatalytic performance for the TiO_2 NTAs due to their reduced electrochemically active areas. The composition of each TiO_2 NTA was determined using energy-dispersive X-ray spectroscopy (EDX), and the results are also shown in Fig. 2. As can be seen the Ti/O ratio gradually increased as the time and voltage of the electrochemical reduction were increased. This result implied that electrochemical reduction should change the conductive properties of TiO_2 and influence the PEC activity of the TiO_2 NTAs.

The capacitance of the TiO_2 NTA and black TiO_2 NTA electrodes was determined using the Mott–Schottky equation:

$$\frac{1}{c^2} = \frac{2}{N_D e \varepsilon_0 \varepsilon} \left(E - E_{FB} - \frac{kT}{e} \right)$$

where c is the capacitance of the space charge layer for the semiconductor, N_D is the carrier density of the electrons, e is the value of the elementary charge, ε_0 is the permittivity of the vacuum, ε is the relative permittivity of the semiconductor, E is the applied bias, E_{FB} is the flatband potential, T is the
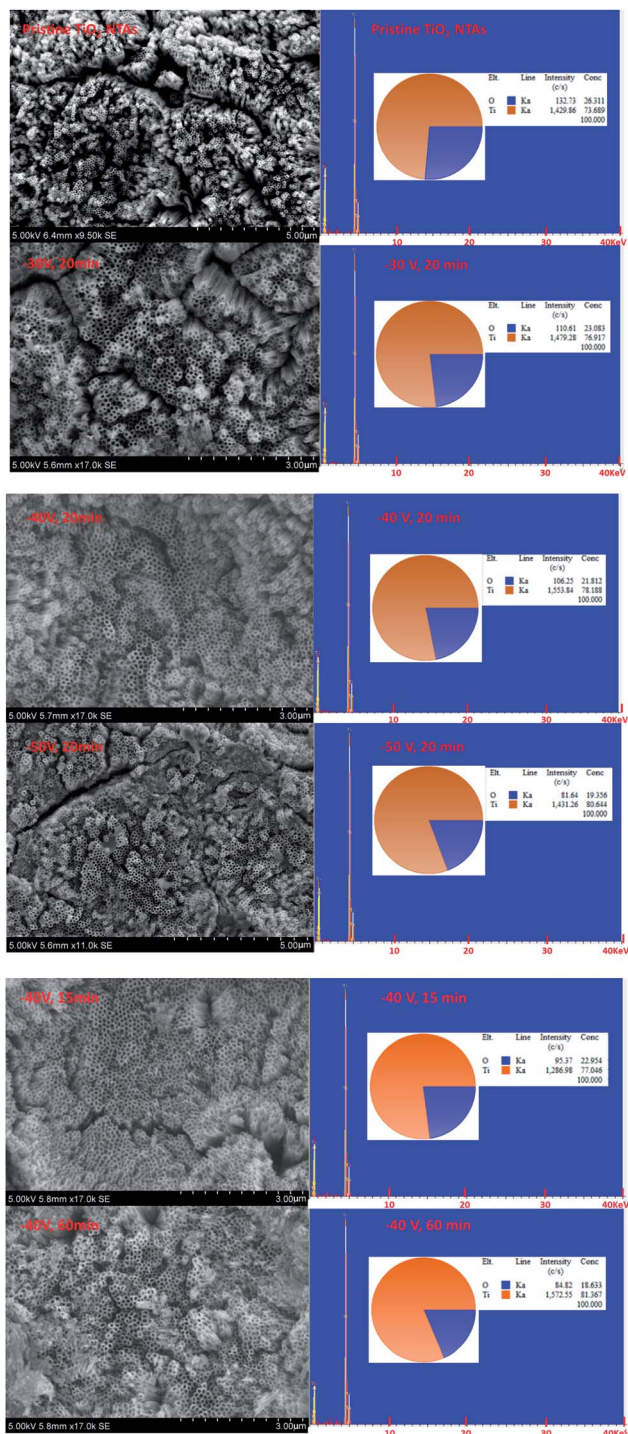
Fig. 2 SEM observation and the corresponding EDX pattern for the pristine TiO$_2$ and black TiO$_2$ NTAs samples.

Fig. 3 Mott–Schottky plots of TiO$_2$ NTAs and black TiO$_2$ NTAs electrodes.

was controlled by the space charge layer.[46] Nevertheless, the black TiO$_2$ NTAs electrode exhibited only a weak correlation between the capacitance and applied potential, which may be attributed to its metallic characteristics.[46] The flatband potentials of the TiO$_2$ NTAs and black TiO$_2$ NTAs were determined to be −0.34 V and −1.07 V, respectively. The more negative E_{FB} of the black TiO$_2$ NTAs could be ascribed to the fact that the presence of Ti^{3+} changed the surface properties of TiO$_2$ due to introducing reduction state,[47,48] enhancing the electrical conductivity of the black TiO$_2$ NTAs.[49] The more negative flatband potential implied that the charge carriers had a high separation rate, because the driving force would be consumed at the flatband potential when electrons are passed through the electrode film. Thus, the more negative E_{FB} of the black TiO$_2$ NTAs electrode is favorable to enhance its electrocatalytic activity.[46,50,51]

Additionally, the N_D value was calculated from the plots in Fig. 3 to evaluate the semiconductor characteristic behavior using the following equation:

Fig. 4 Photocurrent–potential curves of the pristine TiO$_2$ and black TiO$_2$ NTAs electrodes prepared using different electrochemical reduction potentials and times.

temperature, and k is the Boltzmann constant. As seen in Fig. 3, the Mott–Schottky plots of the TiO$_2$ NTAs and black TiO$_2$ NTAs electrodes exhibited a positive slope, which indicated that both coated electrodes are n-type semiconductors. Furthermore, a stronger dependence between the capacity and applied potential was observed in the Mott–Schottky plot of the TiO$_2$ NTAs electrode, which indicated that the capacity of TiO$_2$ NTAs electrode
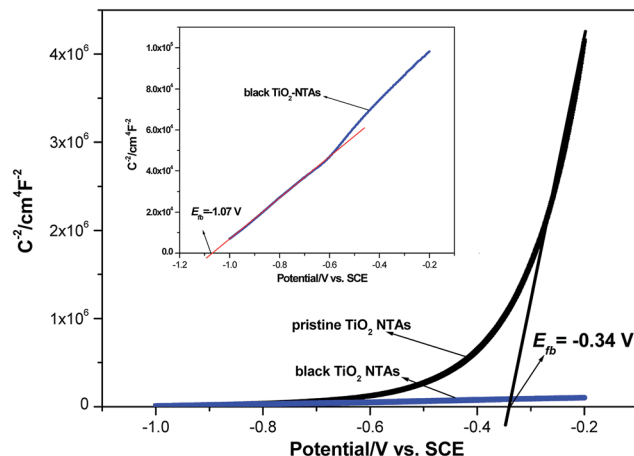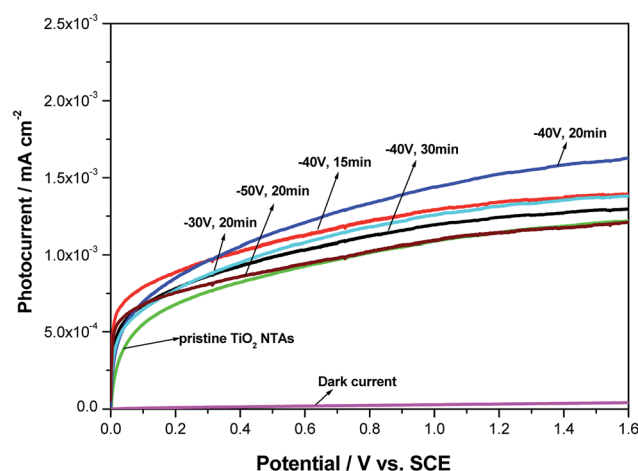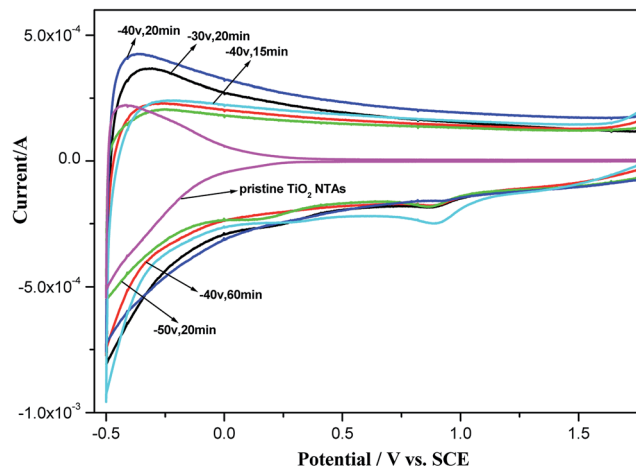
Fig. 5 Cyclic voltammograms of the pristine TiO₂ and black TiO₂ NTA electrodes prepared using different electrochemical reduction potentials and times.

$$N_D = \frac{2}{e \varepsilon_0 \varepsilon} \left(\frac{dE}{d\left(\frac{1}{c^2}\right)} \right)$$

where $e = 1.6 \times 10^{-19}$ C, $\varepsilon_0 = 8.86 \times 10^{-12}$ F m^{-1}, and $\varepsilon = 48$ for anatase TiO₂. Thus, the N_D values for the black TiO₂-NTAs and TiO₂-NTAs were calculated to be 1.25×10^{23} cm^{-3} and 3.0×10^{21} cm^{-3}, respectively. The TiO₂-NTAs showed a low carrier density due to their good semiconducting characteristics. The higher carrier densities of the black TiO₂-NTAs were attributed to an increase in oxygen vacancy states, which act as electron donors.[51] Thus, the black TiO₂ NTAs tend to exhibit higher PEC activity because the higher N_D would lead to lower resistance and promote faster charge transfer.

To investigate the photoelectrochemical behavior of the black TiO₂ NTA electrodes prepared using various reduction potentials and times, current–voltage measurements were

carried out in a 0.2 M Na₂SO₄ solution under solar-light illumination. The LSV photocurrent responses of the different photoelectrodes (see Fig. 4) indicated that the dark-current response of the black TiO₂ NTA electrodes was negligible, which indicated that no electrochemical oxidation occurred. However, a notable enhancement of the photocurrent was observed for all photoelectrodes under illumination, and the photocurrent was potential-dependent. The high photocurrent of the semiconductor reflected the high separation and transfer efficiency of photogenerated charge carriers.[52] As shown in Fig. 4, the black TiO₂ NTA electrodes showed higher photocurrent density than the TiO₂ NTA reference. This result indicated that the black TiO₂ NTA electrodes have higher separation and transfer efficiency of photogenerated carriers than the TiO₂ NTA reference.

To evaluate the electrochemical properties of the black TiO₂ NTAs, cyclic voltammograms were recorded in a 0.5 M Na₂SO₄ aqueous solution. As shown in Fig. 5, the TiO₂ NTA curve showed a strong correlation between the current and potential due to their n-type semiconductor properties. The high resistances of the TiO₂ NTAs at higher potentials led to a decrease in the current, resulting in the pinched shape of the curve. In contrast with the TiO₂ NTAs, the black TiO₂ NTA samples exhibited capacitive curves with rectangular shapes.[28,53] A large, rectangular *CV* curve is clearly observed for the black TiO₂ NTA electrodes at higher current, which indicated that the black TiO₂ NTA samples had high conductivity.[27] The enhanced conductivity of the black TiO₂ NTA can be attributed to the trapped electrons at the Ti³⁺ sites generated by cathodic polarization.[39,40]

As reported in the previous studies,[32–34] amount of ˙OH (from the electro-catalytic decomposition of water on the electrode surface) could be detected using the analysis of the fluorescence spectra (benzoic acid had a known reaction with ˙OH in aqueous media and the product is *p*-hydroxybenzoic acid (*p*-HBA). The *p*-HBA could be detected using fluorescence spectroscopy). To investigate amount of hydroxyl radical (˙OH), the
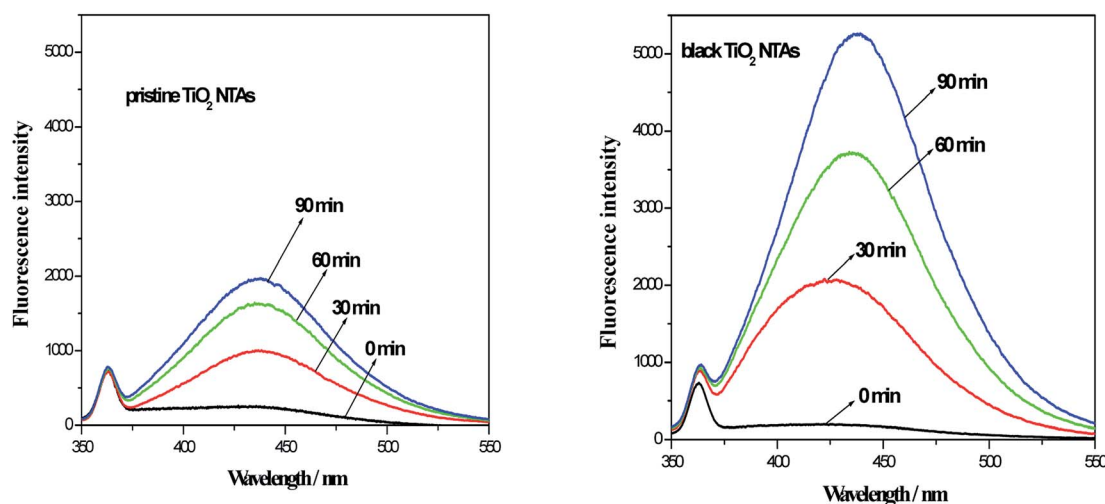

Fig. 6 Fluorescence spectra of the TiO₂ NTA and black TiO₂ NTA electrodes during the photoelectrolysis of benzoic acid (200 mg L^{-1} benzoic acid and 0.5 mol L^{-1} Na₂SO₄ as a supporting electrolyte).
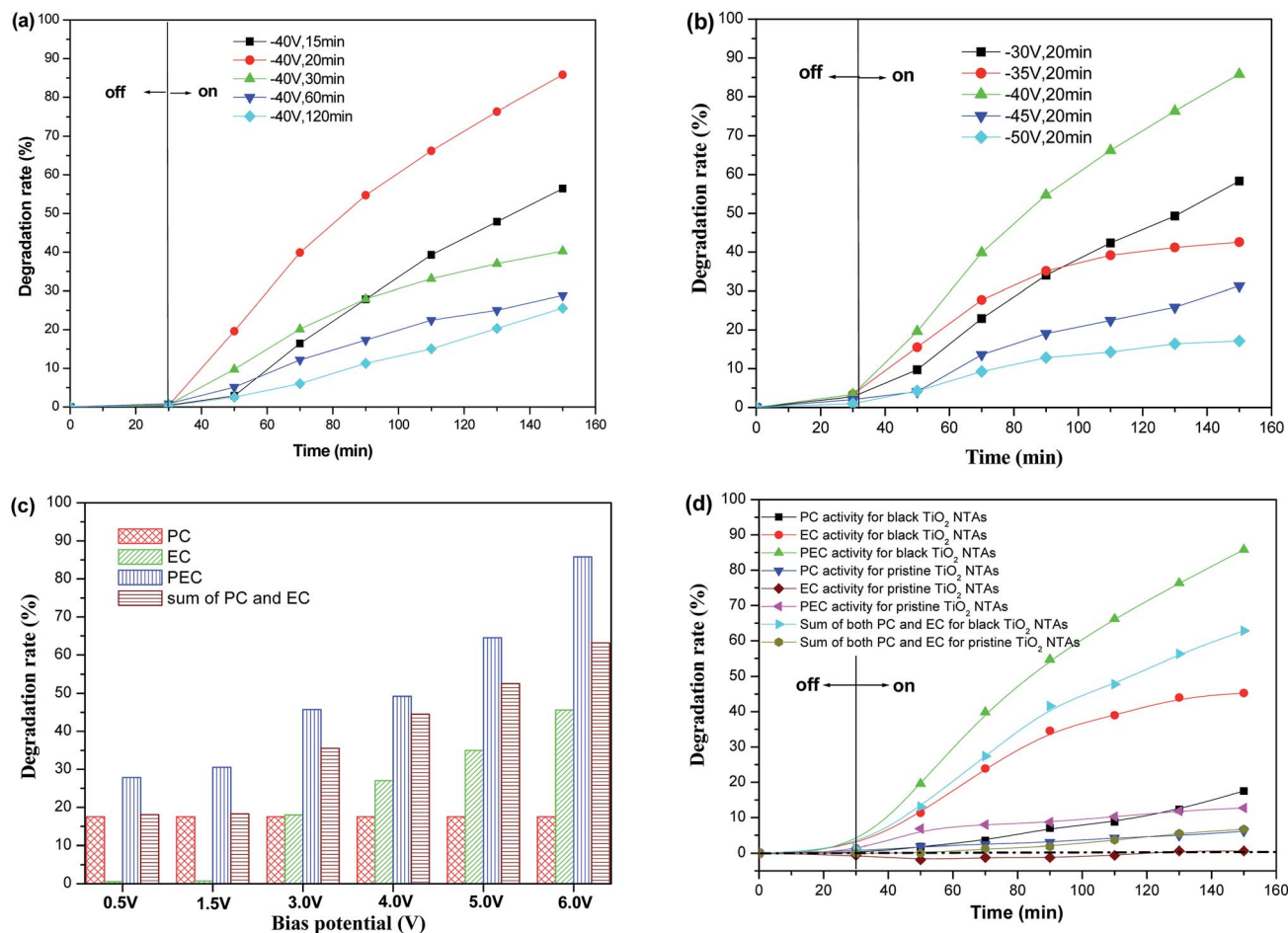
Fig. 7 (a and b) Decolorization efficiencies of KN-R over the black TiO$_2$ NTA electrodes prepared using different electrochemical reduction potentials and times (c) effect of the applied bias on the degradation rate of KN-R over the black TiO$_2$ NTA electrodes (d) efficiencies of the different degradation processes of KN-R over the TiO$_2$ NTAs and black TiO$_2$ NTA electrodes.

electrolysis of benzoic acid solution was performed in present work. Initial concentration of benzoic acid is 200 mg L^{-1} and 0.5 mol L^{-1} Na$_2$SO$_4$ was used as a supporting electrolyte. During electrolysis, the sample was collected and analyzed at a desired time interval. The fluorescence intensity of solution was measured at 440 nm with excitation at 325 nm by a fluorescence spectrophotometer. Fig. 6 shows the photoluminescence (PL) spectra for the photoelectrolysis of the benzoic acid solution over the TiO$_2$ NTA and black TiO$_2$ NTA electrodes. As seen in Fig. 6, the fluorescence intensity of the black TiO$_2$ NTA electrodes was higher than that of the TiO$_2$ NTA electrode at all times, indicating that the black TiO$_2$ NTA electrodes generated more ˙OH. The PL results demonstrated that the black TiO$_2$ NTAs had better current efficiency for the generation of hydroxyl radicals. Obviously, the higher efficiency for the generation of hydroxyl radicals was favorable for the photoelectrocatalytic degradation of organic pollutants.

The photo-electrocatalytic (PEC) degradation efficiency of KN-R over the black TiO$_2$ NTA electrodes prepared using different reduction potentials and times was investigated, as shown in Fig. 7a and b. The degradation rate of KN-R over the black TiO$_2$ NTA electrodes depended on the reduction voltage and time; and the black TiO$_2$ NTA electrode prepared at −40 V

for 20 min exhibited the highest KN-R removal ability. However, excessive electrochemical reduction treatment markedly damaged the pore structure of the TiO$_2$ NTAs, which resulted in a decline in the catalytic performance of the TiO$_2$ NTA electrodes. The effect of the anodic potential on the PEC
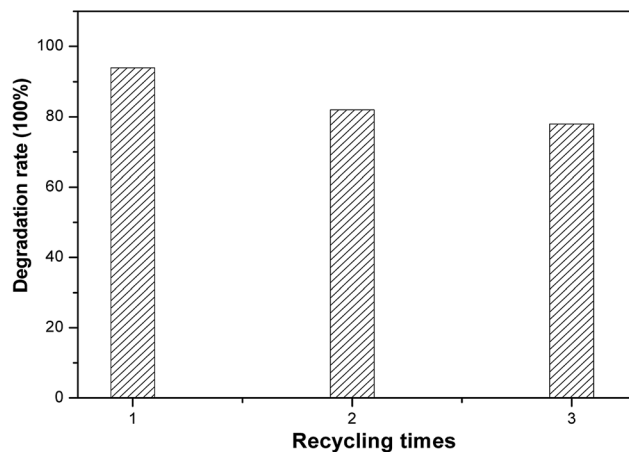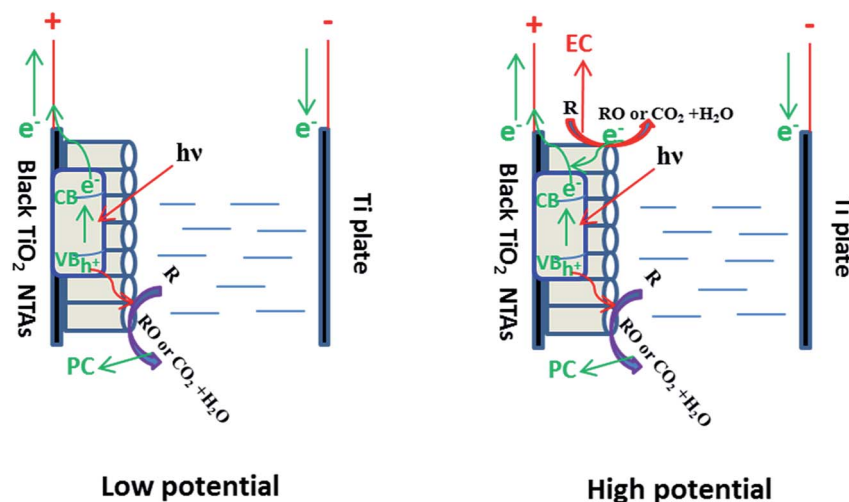

Fig. 8 Results of the recycling experiments for the black TiO$_2$ NTA electrodes for three cycles.

Scheme 1 Diagram of the PEC process over the black TiO_2 NTA electrode under solar light irradiation.

performance of the black TiO_2 NTAs for the degradation of KN-R was also investigated. As shown in Fig. 8c, the PEC degradation rate increased gradually with increasing anodic bias in the potential range of 0–6.0 V. Furthermore, to explore the effect of electro-oxidation on the KN-R removal, a set of pure electro-oxidation measurements were carried out by applying an anodic bias (0–6.0 V) in dark conditions. The electrochemical oxidation of KN-R was not observed when the anodic potential was lower than 3.0 V. However, the electrochemical oxidation of KN-R was non-negligible when the anodic potential was greater than 3.0 V, and KN-R degradation was significantly enhanced at higher potentials. A similar phenomenon was observed in previous work.[54] Fig. 7d shows the degradation rates under various degradation conditions (the electrocatalytic (EC), photocatalytic (PC) and photo-electrocatalytic (PEC) processes) for the black TiO_2 NTAs prepared at −40 V for 20 min. As shown in Fig. 7d, the PEC degradation rate of KN-R over the black TiO_2 NTAs electrode was larger than the sum of both the EC and PC rates, which suggested that an obvious synergetic effect occurred during the PEC process for the black TiO_2 NTAs electrode. The black TiO_2 NTAs electrode exhibited considerable electrocatalytic oxidation of KN-R due to the excellent electrochemical characteristics of the black TiO_2 NTAs. For comparison, the degradation rate of the TiO_2 NTAs electrode was also measured under PEC, EC and PC conditions. Fig. 7 shows that a significant synergetic effect also existed in the PEC process for the TiO_2 NTAs electrode. However, the TiO_2 NTAs electrode did not demonstrate electrocatalytic degradation of KN-R at an anodic potential of 6.0 V. Based on the above results, it can be demonstrated that the black TiO_2 NTAs exhibited better PEC, EC and PC performances than the TiO_2 NTAs.

Based on the above results, a schematic of the PEC process on the black TiO_2 NTAs is illustrated in Scheme 1. When anodic potential is lower than 3.0 V (greater than the flatband potential of the black TiO_2 NTAs), only photocatalytic degradation occurred during the PEC process. Thus, the enhancement of KN-R degradation under these conditions was mainly a result of charge separation by the electric field (electro-assisted

photocatalysis). When the anodic potential was increased above 3.0 V, both photocatalytic and electrochemical degradation for KN-R occurred during the PEC process. In this case, the enhancement of KN-R degradation resulted mainly from the combination of electro-oxidation and electro-photocatalysis.

The service life of electrodes is a significant factor for their practical application. To estimate the electrochemical stability of black TiO_2 NTA electrodes, recycling tests of the degradation of KN-R were carried out under solar light radiation, as shown in Fig. 8. The black TiO_2 NTA electrode still exhibited a considerable removal rate (about 78%) for reactive brilliant blue KN-R after three cycles. The above results indicated that the black TiO_2 NTAs can be used as an excellent PEC electrode.

4. Conclusions

In summary, highly oriented black TiO_2 NTA photoanodes were fabricated using an anodization-electrochemical reduction approach. The as-obtained photoanodes showed stronger light absorption throughout the entire UV-Vis region, a more negative flatband potential, and better separation and transfer efficiency of photoinduced carriers than a conventional TiO_2 NTA electrode. It was found that the photo-electrocatalytic removal of KN-R on black TiO_2 NTA electrodes can be divided into two regimes, namely, electro-assisted photocatalysis at low bias and a combination of electro-assisted photocatalysis and electrochemical oxidation at high bias. The black TiO_2 NTA electrode prepared by electrochemical reducing at −40 V for 20 min, exhibited a highest rate of KN-R degradation. This may be ascribed to the compromise action of conductivity and pore structure for black TiO_2 NTAs under electrochemical reduction. Obviously, the black TiO_2 NTAs can be suggested as a potential cost effective anode material in the field for treatment organic wastewater.

Conflicts of interest

There are no conflicts to declare.

Acknowledgements

References

1 X. Quan, X. L. Ruan, H. M. Zhao, S. Chen and Y. Z. Zhao, *Environ. Pollut.*, 2007, **147**, 409–414.

2 X. Quan, S. G. Yang, X. L. Ruan and H. M. Zhao, *Environ. Sci. Technol.*, 2005, **39**, 3770–3775.

3 J. M. Macak, M. Zlamal, J. Krysa and P. Schmuki, *Small*, 2007, **3**, 300–304.

4 S. P. Albu, A. Ghicov, J. M. Macak, R. Hahn and P. Schmuki, *Nano Lett.*, 2007, **7**, 1286–1289.

5 H. F. Zhuang, C. J. Lin, Y. K. Lai, L. Sun and J. Li, *Environ. Sci. Technol.*, 2007, **41**, 4735–4740.

6 R. Genc, M. O. Alas, E. Harputlu, S. Repp, N. Kremer, M. Castellano, S. G. Colak, K. Ocakoglu and E. Erdem, *Sci. Rep.*, 2017, **7**, 11222.

7 S. Repp, E. Harputlu, S. Gurgen, M. Castellano, N. Kremer, N. Pompe, J. Wörner, A. Hoffmann, R. Thomann, F. M. Emen, S. Weber, K. Ocakoglu and E. Erdem, *Nanoscale*, 2018, **10**, 1877–1884.

8 L. Sun, J. Li, C. L. Wang, S. F. Li, H. B. Chen and C. J. Lin, *Sol. Energy Mater. Sol. Cells*, 2009, **93**, 1875–1880.

9 J. Y. Li, N. Lu, X. Quan, S. Chen and H. M. Zhao, *Ind. Eng. Chem. Res.*, 2008, **47**, 3804–3808.

10 J. Li, H. Yun and C. J. Lin, *J. Electrochem. Soc.*, 2007, **154**, C631–C637.

11 E. Erdem, K. Kiraz, M. Somer and R. A. Eichel, *J. Eur. Ceram. Soc.*, 2010, **30**, 289–293.

12 H. Rumpf, H. Modrow, J. Hormes, H. J. Gläsel, E. Hartmann, E. Erdem, R. Böttcher and K. H. Hallmeier, *J. Phys. Chem. B*, 2001, **105**, 3415–3421.

13 Y. H. Tseng, I. G. Chang, Y. A. Tai and K. W. Wu, *J. Nanosci. Nanotechnol.*, 2012, **12**, 416–422.

14 K. Awazu, M. Fujimaki, C. Rockstuhl, J. Tominaga, H. Murakami, Y. Ohki, N. Yoshida and T. Watanabe, *J. Am. Chem. Soc.*, 2008, **130**, 1676–1680.

15 T. Yamaguchi, E. Kazuma, N. Sakai and T. Tatsuma, *Chem. Lett.*, 2012, **41**, 1340–1342.

16 M. Ye, J. Gong, Y. Lai, C. Lin and Z. Lin, *J. Am. Chem. Soc.*, 2012, **134**, 15720–15723.

17 Z. C. Lian, W. C. Wang, S. N. Xiao, X. Li, Y. Y. Cui, D. Q. Zhang, G. S. Li and H. X. Li, *Sci. Rep.*, 2015, **5**, 10461–10471.

18 K. P. Xie, L. Sun, C. L. Wang, Y. K. Lai, M. Y. Wang, H. B. Chen and C. J. Lin, *Electrochim. Acta*, 2010, **55**, 7211–7218.

19 C. L. Wang, L. Sun, H. Yun, J. Li, Y. K. Lai and C. J. Lin, *Nanotechnology*, 2009, **20**, 295601–295606.

20 Y. Hou, X. Y. Li, X. J. Zou, X. Q. An and G. H. Chen, *Environ. Sci. Technol.*, 2009, **43**, 858–863.

21 G. P. Dai, J. G. Yu and G. Liu, *J. Phys. Chem. C*, 2011, **115**, 7339–7346.

22 Y. B. Xie, L. M. Zhou and H. T. Huang, *Mater. Lett.*, 2006, **60**, 3558–3560.

23 Z. H. Zhang, Y. Yuan, G. Y. Shi, Y. J. Fang, L. H. Liang, H. C. Ding and L. T. Jin, *Environ. Sci. Technol.*, 2007, **41**, 6259–6263.

24 N. Alberto, A. Mattia, S. Saveria, M. Marelli, F. Fabbri, S. Cappelli, C. L. Bianchi and R. Psaro, *J. Am. Chem. Soc.*, 2012, **134**, 7600–7603.

25 N. Liu, C. Schneider, D. Freitag, M. Hartmann, U. Venkatesan, J. Muller, E. Spiecker and P. Schmuki, *Nano Lett.*, 2014, **14**, 3309–3313.

26 H. L. Cui, W. Zhao, C. Y. Yang, H. Yin, T. Q. Lin, Y. F. Shan, Y. Xie, H. Gu and F. Q. Huang, *J. Mater. Chem. A*, 2014, **2**, 8612–8616.

27 C. Kim, S. Kim, J. Choi, J. Lee, J. S. Kang, Y. E. Sung, J. Lee, W. Choi and J. Yoon, *Electrochim. Acta*, 2014, **141**, 113–119.

28 C. Kim, S. Kim, J. Lee, J. Kim and J. Yoon, *ACS Appl. Mater. Interfaces*, 2015, **7**, 7486–7491.

29 A. Q. Zhang, F. L. Gong, Y. H. Xiao, X. P. Guo, F. Li, L. Z. Wang, Y. Zhang and L. S. Zhang, *J. Electrochem. Soc.*, 2017, **164**(2), H91–H96.

30 H. Wu, D. Li, X. Zhu, C. Yang, D. Liu, X. Chen, Y. Song and L. Lu, *Electrochim. Acta*, 2014, **116**, 129–136.

31 Q. Zheng, H. J. Lee, J. Lee, W. Choi, N. B. Park and C. Lee, *Chem. Eng. J.*, 2014, **249**, 285–292.

32 M. E. Lindsey and M. A. Tarr, *Chemosphere*, 2000, **41**, 409–417.

33 M. L. And and M. A. Tarr, *Environ. Sci. Technol.*, 2000, **34**, 444–449.

34 W. H. Yang, W. T. Yang and X. Y. Lin, *Acta Phys.-Chim. Sin.*, 2012, **28**, 831–836.

35 E. Erdem, P. Jakes, R. A. Eichel, D. C. Sinclair, M. Pasha and I. M. Reaney, *Funct. Mater. Lett.*, 2010, **3**, 65–68.

36 J. G. Yu, H. G. Yu, B. Cheng, X. J. Zhao, J. C. Yu and W. K. Ho, *J. Phys. Chem. B*, 2003, **107**, 13871–13879.

37 H. M. Zhu, B. F. Yang, J. Xu, Z. P. Fu, M. W. Wen, T. Guo, S. Q. Fu, J. Zuo and S. Y. Zhang, *Appl. Catal., B*, 2009, **90**, 463–469.

38 X. X. Yu, J. G. Yu, B. Cheng and M. Jaroniec, *J. Phys. Chem. C*, 2009, **113**, 17527–17535.

39 J. M. Macak, B. G. Gong, M. Hueppe and P. Schmuki, *Adv. Mater.*, 2007, **19**, 3027–3031.

40 F. Fabregat-Santiago, E. M. Barea, J. Bisquert, G. K. Mor, K. Shankar and C. A. Grimes, *J. Am. Chem. Soc.*, 2008, **130**, 11312–11316.

41 S. S. M. Lu, F. H. Pollak and P. M. Raccah, *Phys. Rev. B*, 1978, **17**, 1970–1975.

42 G. K. Mor, O. K. Varghese, M. Paulose and C. A. Grimes, *Adv. Funct. Mater.*, 2005, **15**, 1291–1296.

43 Z. Wang, C. Y. Yang, T. Q. Lin, H. Yin, P. Chen, D. Y. Wan, F. F. Xu, F. Q. Huang, J. H. Lin, X. M. Xie and M. H. Jiang, *Energy Environ. Sci.*, 2013, **6**, 3007–3014.

44 H. Q. Tan, Z. Zhao, M. Niu, C. Y. Mao, D. P. Cao, D. J. Cheng, P. Y. Feng and Z. C. Sun, *Nanoscale*, 2014, **6**, 10216–10223.

45 S. Tominaka, *Chem. Commun.*, 2012, **48**, 7949–7951.

46 R. Hahn, F. Schmidt-Stein, J. Salonen, S. Thiemann, Y. Y. Song, J. Kunze, V. P. Lehto and P. Schmuki, *Angew. Chem., Int. Ed.*, 2009, **48**, 7236–7239.

47 H. Ge, H. Tian, Y. G. Zhou, S. Y. Wu, D. L. Liu, X. Z. Fu, X. M. Song, X. C. Shi, X. X. Wang and N. Li, *ACS Appl. Mater. Interfaces*, 2014, **6**, 2401–2406.

48 H. A. Girard, N. Simon, D. Ballutaud and A. Etcheberry, *C. R. Chim.*, 2008, **11**, 1010–1015.

49 H. Zhou and Y. R. Zhang, *J. Phys. Chem. C*, 2014, **118**, 5626–5636.

50 A. I. Kontos, V. Likodimos, T. Stergiopoulos, D. S. Tsoukleris, P. Falaras, I. Rabias, G. Papavassiliou, D. Kim, J. Kunze and P. Schmuki, *Chem. Mater.*, 2009, **21**, 662–672.

51 G. M. Wang, H. Y. Wang, Y. C. Ling, Y. C. Tang, X. Y. Yang, R. C. Fitzmorris, C. C. Wang, J. Z. Zhang and Y. Li, *Nano Lett.*, 2011, **11**, 3026–3033.

52 H. G. Kim, P. H. Borse, W. Choi and J. S. Lee, *Angew. Chem., Int. Ed.*, 2005, **117**, 4661–4665.

53 H. Li, Z. H. Chen, C. K. Tsang, Z. Li, X. Ran, C. Lee, B. Nie, L. X. Zheng, T. Hung, J. Lu, B. C. Pan and Y. Y. Li, *J. Mater. Chem. A*, 2014, **2**, 229–236.

54 C. He, X. Z. Li, N. Graham and Y. Wang, *Appl. Catal., A*, 2006, **305**, 54–63.